Retrieval of total precipitable water from thermal infrared observations of INSAT-3D imager over the ocean

Rishi Kumar Gangwar* and P. K. Thapliyal

Geophysical-parameter Retrievals Division, Atmospheric and Oceanic Sciences Group, Earth, Ocean, Atmosphere, Planetary Sciences and Applications Area, Space Applications Centre,
Indian Space Research Organisation, Ahmedabad 380 015, India

The present study aims to develop a retrieval algorithm for total precipitable water (TPW) over the ocean using Indian geostationary satellite INSAT-3D observations. The algorithm computes TPW as the sum of two broad layers using thermal infrared observations of the Imager for clear sky and upper tropospheric humidity (UTH) products. First, the differential absorption of the atmospheric water vapour in split-window channels is exploited to estimate atmospheric water vapour concentration from surface to mid-troposphere. Secondly, the contribution from UTH products available from the INSAT-3D Imager is added to estimate TPW. The algorithm performance has been assessed by comparing the INSAT-3D-retrieved TPW with collocated TPW products from radiosonde, INSAT-3D Sounder and Moderate Resolution Imaging Spectroradiometer (MODIS) onboard Aqua satellite for the year 2018. The standard deviation of the error was found to be around 0.5 cm for each of the months.

Keywords: Geostationary satellite, ocean, retrieval algorithm, thermal infrared observations, total precipitable water.

ATMOSPHERIC columnar water vapour, also known as total precipitable water (TPW), plays an important role in studies related to the earth's hydrological cycle, weather and climate monitoring[1,2]. Water vapour is also one of the most significant greenhouse gases, which absorbs the earth's radiative energy. The study of various important atmospheric processes requires the high temporal and spatially distributed observations of water vapour. The high spatio-temporal resolution TPW, together with information on atmospheric stability, is an effective indicator of severe weather phenomena in pre-convective atmospheric condition, occasionally leading to thunderstorms[3,4]. Water vapour, one of the most influential constituents of the atmosphere, is responsible for determining the amount of precipitation that a region can receive[5]. The conventional methods, such as radiosondes from a selected few weather stations, do not provide sufficient observations. Radiosonde provides observations twice a day over selected land-based stations limited to major cities, and is expensive to maintain. These observa-

tions are particularly sparse over oceanic regions. Temporal variations in atmospheric water vapour occur rapidly and water vapour measurements by radiosondes do not satisfy the needs of research for various scales of atmospheric water vapour. In this regard, satellite-based measurements have become a necessity that provide global observations with high spatial and temporal resolution. In addition, knowledge of TPW in the atmosphere is also used for atmospheric correction to improve the accuracy of the retrieved surface parameters such as land and sea surface temperature from satellite observations[6,7]. To achieve this various retrieval techniques have been proposed to estimate atmospheric water vapour from satellite-based observations having thermal infrared split-window channels[8–10]. The split-window logarithm ratio (SWLR) algorithm of Chesters et al.[11] considered that the ratio of brightness temperatures for the split-window channels tends to increase with amount of the TPW. They assumed a single atmospheric layer between 1000 and 600 hPa, and derived the ratio of brightness temperatures in terms of TPW.

India successfully launched its first advanced meteorological satellite, INSAT-3D, in July 2013 in the geostationary orbit at 82°E. Meteorological payloads on-board INSAT-3D are: a six-channel Imager and a 19-channel Sounder mainly for atmospheric profiles of temperature and moisture, cyclone and weather monitoring, cloud motion vectors (CMV), rainfall estimation, snow-cover detection, mesoscale studies, etc. The INSAT-3D Imager has a split-window (TIR1 and TIR2), mid-infrared (IR) (MIR) window, and shortwave IR (SWIR), water vapour (WV) absorption and visible channels. Table 1 provides details of the INSAT-3D Imager channels. The spectral response functions (SRFs) of TIR1/2, MIR and WV bands of INSAT-3D are shown in the Figure 1 along with a sample brightness temperature spectra of the infrared atmospheric sounding interferometer (IASI) for a standard tropical atmosphere.

Currently, the Sounder on-board INSAT-3D provides TPW information computed from the vertical moisture profile estimates, but the temporal resolution is 1 h for a smaller observation region of Indian land mass and the nearby oceanic region. In contrast, the Imager is capable

Table 1. Characteristics of the INSAT-3D Imager channels

Band# (name)	Wavelength (μm)	Resolution (km)	SNR or NEDT
1 (VIS)	0.52–0.72	1	150 : 1
2 (SWIR)	1.55–1.70	1	150 : 1
3 (MIR)	3.80–4.00	4	0.27 K @300 K
4 (WV)	6.50–7.00	8	0.18 K @230 K
5 (TIR1)	10.3–11.2	4	0.10 K @300 K
6 (TIR2)	11.5–12.5	4	0.25 K @300 K

SNR, Signal-to-noise-ratio; NEDT, Noise equivalent differential temperature.

*For correspondence. (e-mail: rgbly1986@sac.isro.gov.in)

of providing observations over a full-disk area every 30 min interval and at a spatial resolution of 4–8 km, far superior compared to the Sounder. The Imager also has a visible channel at spatial resolution of 1 km, thereby helping in detecting fractional cloud cover within a TIR1/2 pixel during day time, leading to an improved clear-sky retrieval of TPW.

The present study describes the development of a retrieval algorithm for TPW estimation from thermal infrared split-window observations and UTH products of the INSAT-3D Imager.

The INSAT-3D Imager observations of brightness temperature in TIR1 and TIR2 channels and operational UTH products have been obtained from the Meteorological and Oceanographic Satellite Data and Archival Centre (MOSDAC) (https://www.mosdac.gov.in), Space Applications Centre (ISRO) for the period January–October 2018. The brightness temperatures of INSAT-3D are regularly inter-calibrated with respect to IASI measurements using Global Space-based Inter-Calibration System (GSICS) procedures. The UTH product is derived from the water vapour channel observations of the Imager[12].

The retrieved TPW products have been validated with a few radiosonde (RS)-derived TPW available from nearby islands. Additionally, TPW product from Moderate Resolution Imaging Spectroradiometer (MODIS) onboard Aqua satellite and INSAT-3D Sounder have also been acquired for extensive quality assessment of the retrieved TPW from INSAT-3D Imager.

Since cloud absorbs most of the radiation in the IR band emitted from the earth's surface, the retrieval of TPW has been performed only for cloud-free regions. In order to detect the cloudy pixels and exclude them from further analysis, the operational cloud mask product of INSAT-3D Imager has been used[12].

It is well known that the water vapour densities are maximum at the lower troposphere, exponentially decreasing to the upper tropospheric layers. Therefore, generally most of the water vapour is found in the lower and mid-tropospheric layers of the atmosphere. Although the split-window-based algorithms estimate most of the

Figure 1. Spectral response functions (SRFs) of infrared channels of INSAT-3D Imager superimposed on IASI brightness temperature (Tb) spectra.

atmospheric water vapour, they do not fully account for the upper tropospheric contribution in TPW. Therefore, in order to obtain the integrated water vapour in the atmospheric column, we propose an algorithm to estimate TPW by combining both the contributions; from the upper troposphere together with the lower to middle troposphere. The lower to middle tropospheric contribution (PW1) is estimated using split-window observations, while the upper troposphere contribution (PW2) is derived from the upper tropospheric humidity products. Finally, TPW can be derived using following expression

$$\text{TPW} = \text{PW1} + \text{PW2}. \tag{1}$$

PW1 is estimated as described below. The split window is designed to exploit the differential absorptions in thermal infrared channels at 11 and 12 μm due to the presence of water vapour in the atmosphere[13]. Chesters et al.[10] suggested the following expression to estimate TPW using split-window observations

$$\text{TPW} = \frac{1}{\Delta\alpha}\left[\frac{1}{\sec\theta}\ln\left(\frac{\text{BT}_{11} - T_{\text{air}}}{\text{BT}_{12} - T_{\text{air}}}\right) - \Delta\kappa\right], \tag{2}$$

where BT_{11} and BT_{12} are the brightness temperatures corresponding to TIR1 and TIR2 channels respectively; T_{air} is the effective atmospheric temperature of the layer from the surface to middle troposphere (~600 hPa) and $\Delta\alpha$ and $\Delta\kappa$ are the absorption coefficients. Chesters et al.[10] assumed a single atmospheric layer up to 600 hPa to compute TPW, excluding the upper tropospheric contribution. Hence, eq. (2) may be considered as a primary contributor (PW1) of eq. (1) in estimating TPW.

Equation (2) is nonlinear but has a well-behaved relationship between the split-window and PW1, scaled by the three atmospheric parameters, viz. $\Delta\kappa$, $\Delta\alpha$ and T_{air}. These three parameters can be determined by applying a numerical least-square minimization procedure with respect to a set of 'ground truth' PW1 values embedded in a region.

Equation (2) has three unknown parameters, viz. $\Delta\kappa$, $\Delta\alpha$ and T_{air} that are required in addition to the INSAT-3D Imager observations for estimating PW1. These parameters are computed using statistical regression technique. Equation (2) can be rewritten as

$$\text{PW1} = a + b\left(\frac{1}{\sec(\theta)}\ln\left[\frac{\text{BT}_{11} - \bar{T}}{\text{BT}_{12} - \bar{T}}\right]\right), \tag{3}$$

where $a = -(\Delta\kappa/\Delta\alpha)$, $b = (1/\Delta\alpha)$ and $\bar{T} = T_{\text{air}}$.

The algorithm parameters such as a, b, and $\bar{T}$ can be determined by least-square fit method using PW1 and corresponding brightness temperatures of the split-window channels, simulated from radiative transfer model[11].
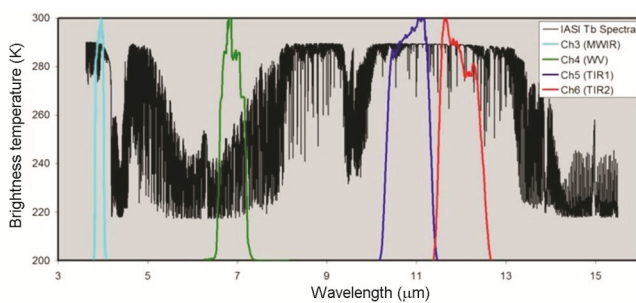
For simulation of the INSAT-3D Imager channel brightness temperatures, Radiative Transfer for Television Infrared Observation Satellite (TIROS) Operational Vertical Sounder (RTTOV)-v11 radiative transfer model has been used. RTTOV-v11 is a fast radiative transfer model originally developed at the European Centre for Medium range Weather Forecast (ECMWF) in the early 1990s for Television Infrared Operational Satellite (TIROS) Operational Vertical Sounder (TOVS)[14]. Subsequently, the original code has gone through several developments[15,16], more recently, within the EUMETSAT NWP Satellite Application Facility (SAF). The atmospheric profiles and required surface variables have been taken from ECMWF diverse datasets[17]. The simulations have been performed for clear atmospheres over the oceanic region spanning from 0° to 130°E and 60°S to 60°N only, corresponding to the full disk-viewing region of INSAT-3D and for satellite zenith angle varying from 0° to 60°.

Considering an arbitrary value of $\bar{T}$ and using the simulated brightness temperatures of INSAT-3D TIR1 and TIR2 channels, we have applied statistical regression on eq. (3) and computed the values of $a = 0.49$ cm and $b = 42.44$ cm.

Now, using the above values of a and b in eq. (3), PW1 is retrieved using simulated brightness temperatures for different values of $\bar{T}$ and then compared with the actual PW1. The best estimated value of PW1 gives the optimized value of $\bar{T}$, which was found to be 260 K (Figure 2).

Therefore, the optimized values of the parameters to retrieve PW1 from the INSAT-3D Imager observations are: $a = 0.49$ cm, $b = 42.44$ cm and $\bar{T} = 260$ K.

A simulation-based sensitivity study was carried out for noise in brightness temperature observations in TIR1 and TIR2 channels to analyse the errors in the retrieved PW1. The simulations have been performed with RTTOV radiative transfer model using atmospheric profiles from ECMWF diverse training dataset for INSAT-3D Imager channels. Figure 3 shows the impact of noise in both the channels on the retrieved PW1. It can be clearly seen that if both the channels have larger noise, the error in the retrieved PW1 increases significantly. For the INSAT-3D noise values given Table 1, the theoretical error in PW1 estimation is found to be 0.63 cm.

PW2 is computed using INSAT-3D-derived UTH products. UTH is a measure of the weighted mean relative humidity according to the weighting function of the water vapour channel[18]. Therefore, UTH from the INSAT-3D Imager is a representative of the relative humidity around the atmospheric layer from 600 to 300 hPa, because the weighting function of its water vapour channel peaks around 450 hPa. Relative humidity of this layer is converted into specific humidity using atmospheric temperature values from 600 to 100 hPa, taken from Global Forecast Systems (GFS) forecast fields. Further,

by integrating the specific humidity values, the precipitable water corresponding to UTH, i.e. PW2 is estimated.

To evaluate its performance, the developed retrieval algorithm has been applied on 10 months' (January–October 2018) data of split-window observations as well as UTH products of the INSAT-3D Imager to retrieve TPW. The retrieved TPW has been compared with the collocated TPW products available from RS measurements, MODIS and the INSAT-3D Sounder. Moreover, the microwave sensor-derived TPW has coarser spatial resolution (~25 km) compared to the INSAT-3D TPW. Therefore, we did not compare with microwave TPW. To quantify the retrieval errors, the standard statistical parameters, viz. mean (bias) and standard deviation of the differences (Std) were computed.

As the developed retrieval algorithm provides TPW over the oceans only, very few RS measurements (four stations) could be acquired on neighbouring islands.
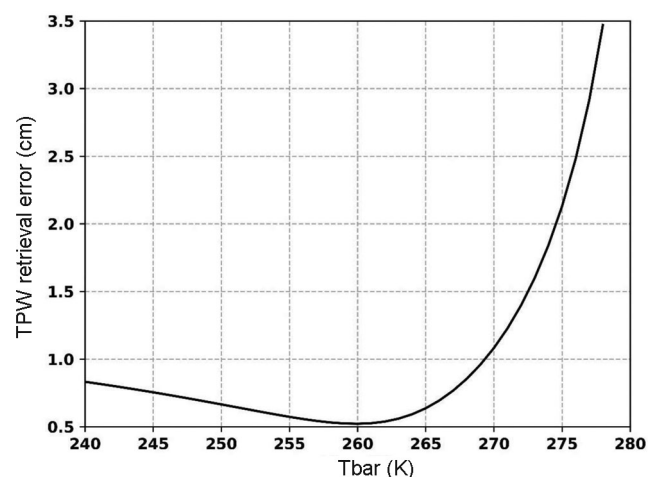

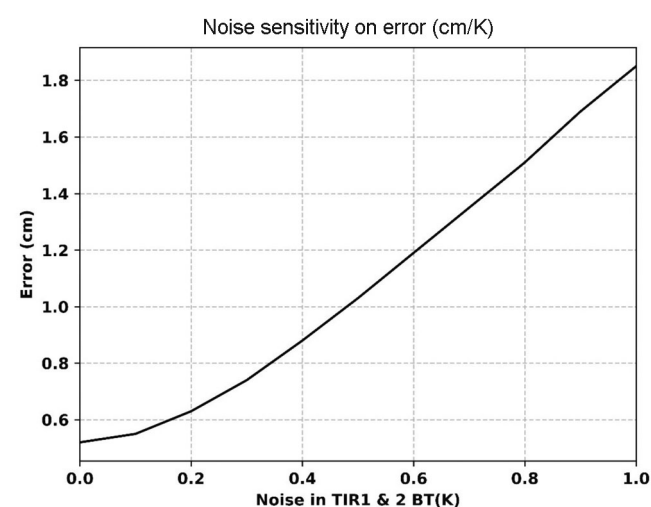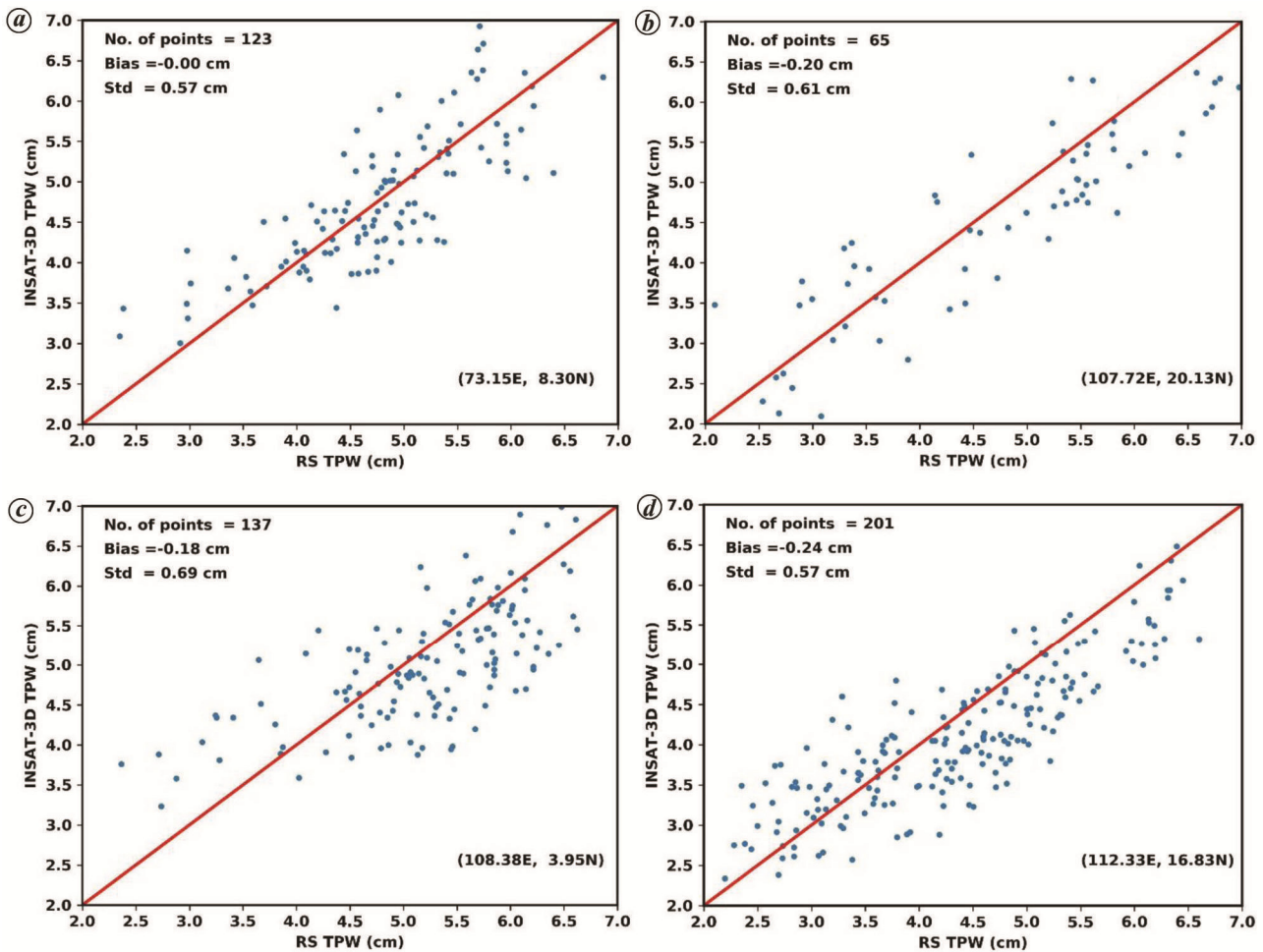**Figure 2.** Computation of $\bar{T}$.

Figure 3. Noise sensitivity of retrieval error.

Figure 4. Scatter plots of INSAT-3D TPW versus RAOB TPW for January–October 2018 at locations. *a*, 73.15E, 8.3N; *b*, 107.72E, 20.13N; *c*, 108.38E, 3.95N; *d*, 112.33E, 16.83N.

Therefore, validation was performed with four radiosonde observations measured at (73.15E, 8.30N), (107.72E, 20.13N), (108.38E, 3.95N) and (112.33E, 16.83N). The RS observations were acquired from upper air sounding portal of the University of Wyoming, USA (www. weather.uwyo.edu/sounding.html). The closest INSAT-3D TPW pixel found within 10 km radius centred around each RS location and time difference of 30 min was considered as a collocation criterion. Figure 4 *a–d* shows the scatter plots for each RS location for the entire period. The corresponding statistical parameters are also shown in the figure.

To examine the spatial and seasonal variations in the retrieved INSAT-3D TPW products, the collocated TPW products from Aqua-MODIS were used (http://ladsweb. modaps.eosdis.nasa.gov). The MODIS TPW products generated from infrared algorithm (MYD07) were used for comparison because of their day–night availability[19]. The other MODIS TPW products from near-infrared algorithm (MYD05) are available only during daytime. In addition, the spatial resolution (5 km × 5 km) of the

MYD07 products is closer to the INSAT-3D-derived products (8 km × 8 km) compared to the MYD05 products (1 km × 1 km).

The spatial distributions of TPW are shown in Figure 5 *a–l* for January, April, July and October, to depict seasonal variations. The spatial distribution of MYD07 products are also shown for qualitative comparison.

The spatial resolution of 0.05° and temporal resolution of ±15 min are considered as a collocation criterion for computing the comparison statistics between both products.

From Figure 5, it can be observed that both retrieved TPW and MYD07 TPW show similar spatial distribution. The high concentration of TPW along the equatorial ocean demonstrates the ability of this algorithm to capture the actual distribution of TPW. The shift in the high concentration region towards north from January to July shows the seasonal changes that occur in TPW.

Figures 5 *d–i* shows an increase in TPW values over the Arabian Sea during April to July. This enhancement, in general, make the conditions favourable for the onset
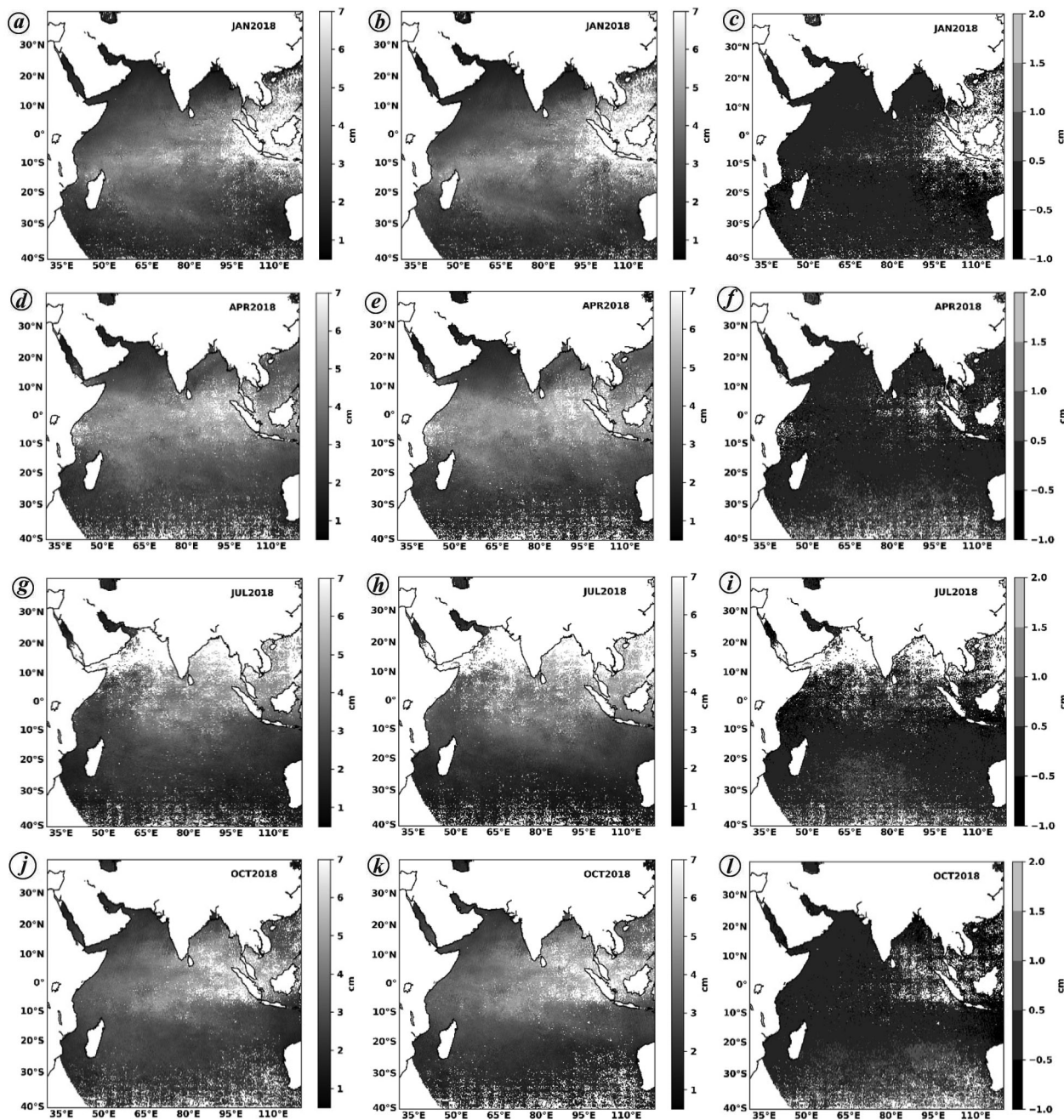
Figure 5. Spatial distribution of TPW for January 2018: *a*, INSAT-3D; *b*, MODIS; *c*, INSAT-3D – MODIS, April; *d*, INSAT-3D; *e*, MODIS; *f*, INSAT-3D – MODIS, July; *g*, INSAT-3D; *h*, MODIS; *i*, INSAT-3D – MODIS, October; *j*, INSAT-3D; *k*, MODIS; *l*, INSAT-3D – MODIS.

of the Indian summer monsoon. Simon *et al.*[20] monitored monsoon onset over the Kerala coast using TPW from Tropical Rainfall Measuring Mission (TRMM) Microwave Imager (TMI). They further showed that water vapour over the western Arabian Sea region is an important parameter that provides us with a lead time of two and half weeks for predicting monsoon onset over Kerala.

Moreover, Figure 5 also show the differences between INSAT-3D-retrieved TPW and MYD07 TPW products along with the spatial plots. The difference plots provide the error distribution in the retrieved TPW. There are

very small regions that show higher differences, i.e. more than 0.5 cm, indicating overall good performance of the present retrieval algorithm.

To quantify the retrieval errors, bias and Std have been computed at monthly scales. Figure 6 provides the monthly statistics computed in TPW with respect to MYD07 products along with density scatter plots. Figure 6 *a–d* shows a comparison of TPW versus MYD07 TPW for four months, viz. January, April, July and October 2018, representing different seasons, viz. winter, summer, monsoon and spring respectively.
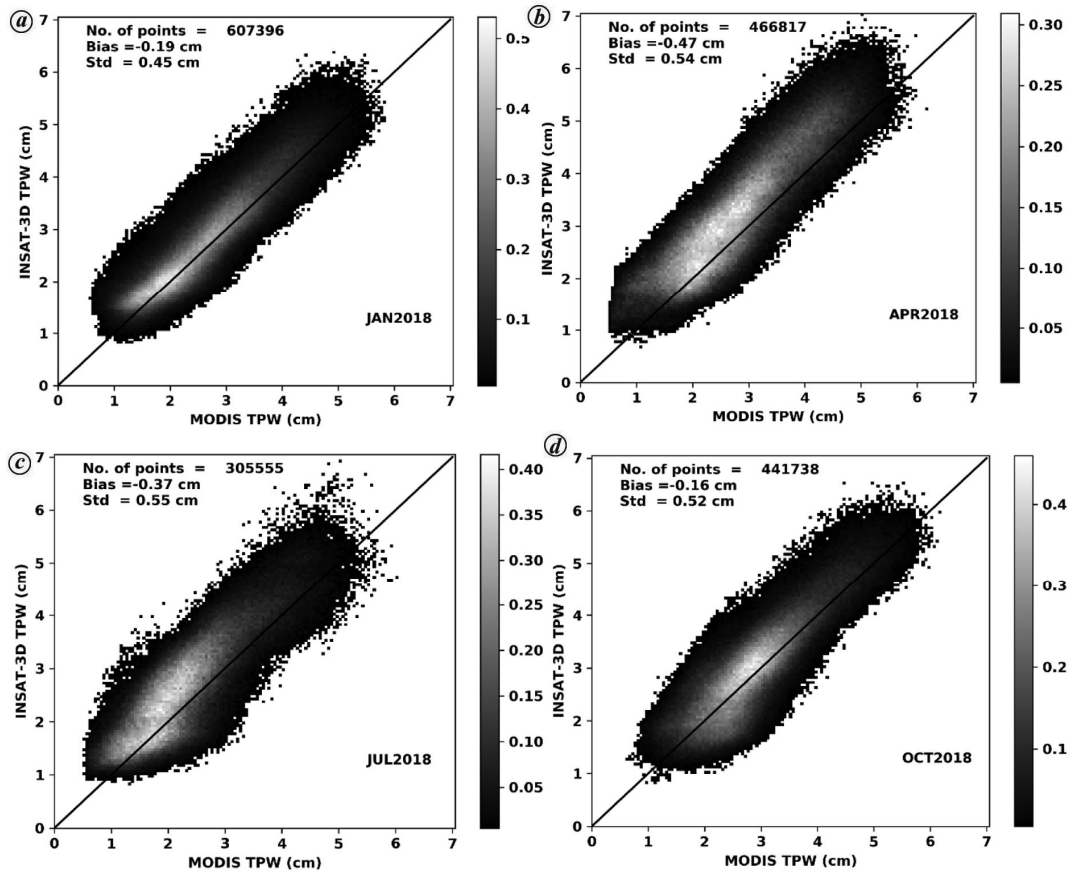
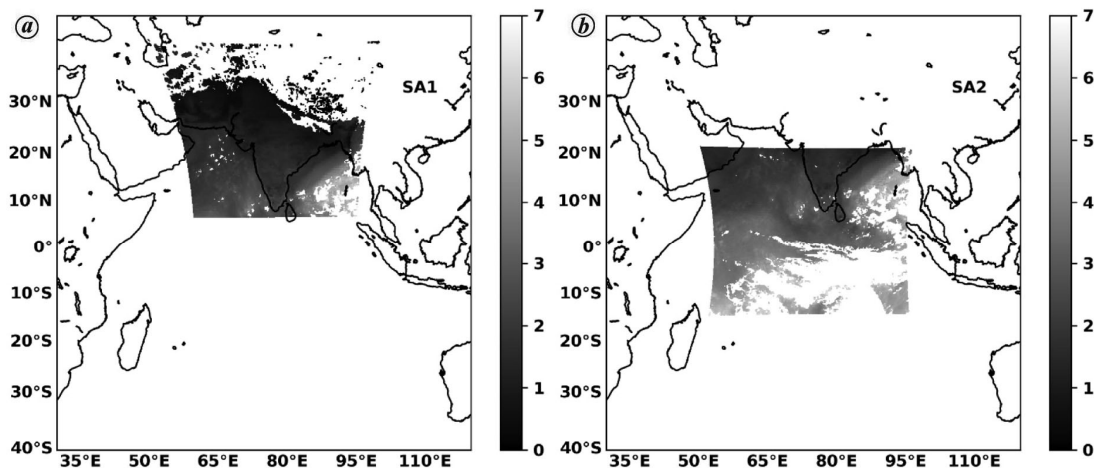**Figure 6.** Density scatter plot of INSAT-3D versus MODIS for 2018: *a*, January; *b*, April; *c*, July; *d*, October.

Figure 7. Typical INSAT-3D Sounder TPW products for (*a*) SA1 and (*b*) SA2 regions.

The INSAT-3D Sounder provides TPW every hour primarily over the Indian landmass (sector SA1) and every 6 h over the Indian Oceanic region (sector SA2, Figure 7). TPW has been estimated by integrating the retrieved moisture profiles from sounder observations in thermal infrared channels[12]. The quality assessment of sounder TPW products was performed by Parihar *et al.*[21], and Rao *et al.*[22]. The former group found root mean square error of 0.8 cm when compared with RS observa-

tions on daily and monthly scales[21]. The latter group compared the Atmospheric Infrared Sounder (AIRS) TPW and Global Navigational Satellite System (GNSS)-observed TPW, and reported performance degradation during June to August over coastal regions of the Arabian Sea and Bay of Bengal[22].

As the INSAT-3D Sounder provides hourly TPW over land and every six hourly over the ocean, we have performed the retrieval over oceanic regions only. For
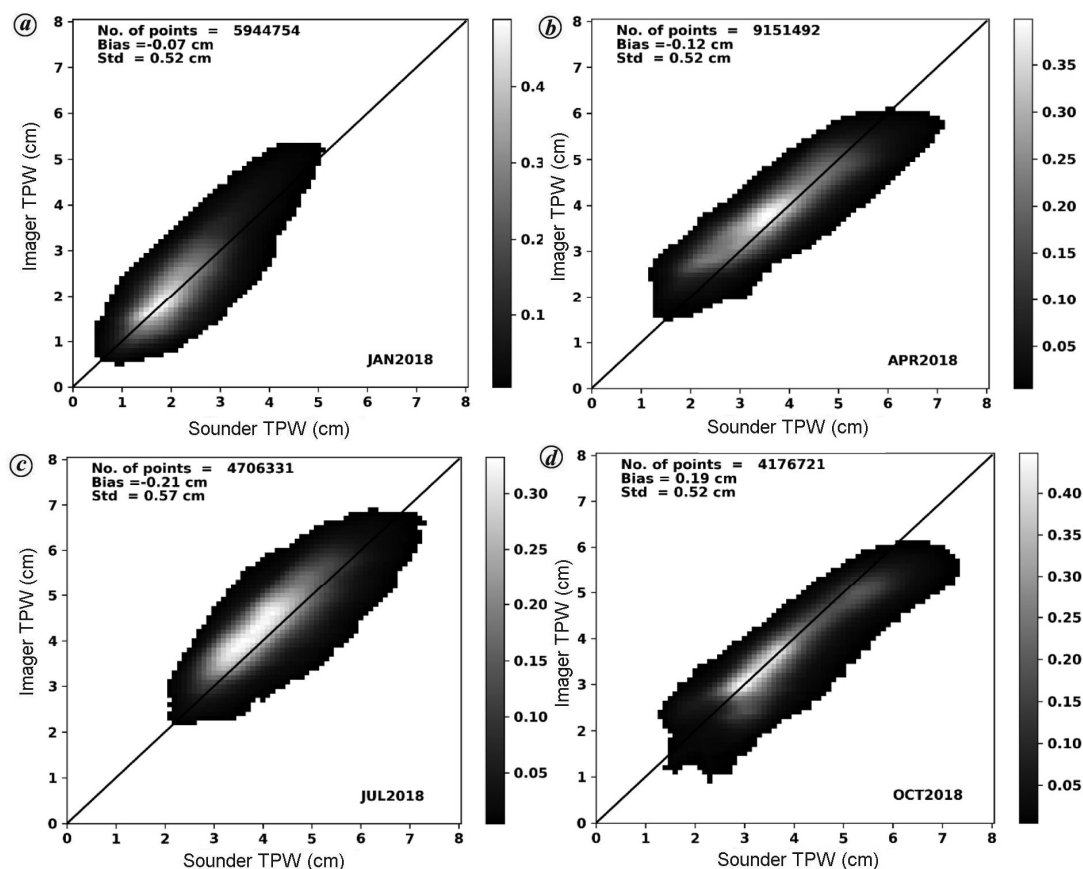
Figure 8. Density scatter plots of INSAT-3D Imager and Sounder TPW on a monthly scale for 2018: *a*, January; *b*, April; *c*, July; *d*, October.
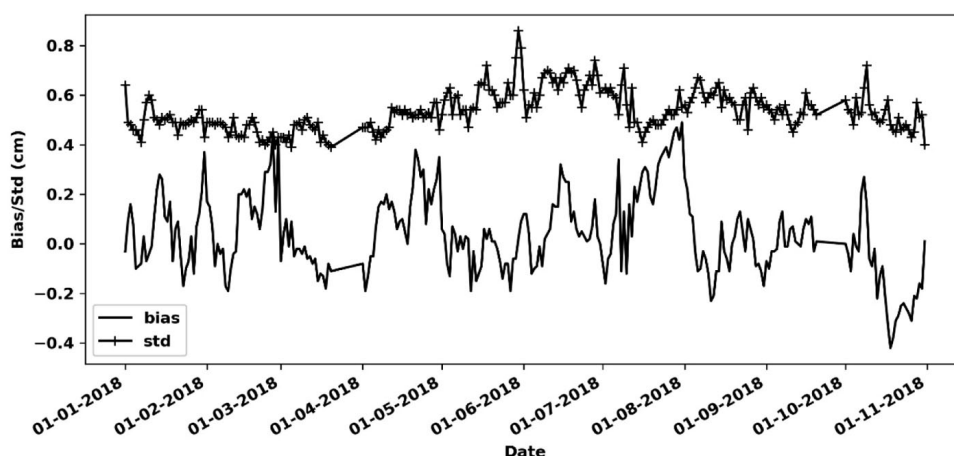

Figure 9. Time series of daily bias and standard (Std) deviation of the differences between INSAT-3D Imager and Sounder TPW for January–October 2018.

collocating these two products, spatial resolution of 0.1° and temporal resolution of ±15 min was used.

The density scatter plots were generated on monthly scales to characterize the distribution in different bins of TPW (Figure 8). The monthly biases and standard deviation of differences are also provided in the figure. A Std of ~0.5 cm is observed in all months with slight underestimation in TPW, except in October.

Figure 9 shows the comparison statistics generated on daily scale for the entire period of validation. The daily Std is less than 0.6 cm, except for a few weeks during monsoon season. The slightly large error in the monsoon season can be attributed to cloud cover persistence over most of the Indian region. So the cloud contamination of the observation is greater in the monsoon season. Another reason may be the degraded performance of the

Sounder TPW in the monsoon season, as reported by Rao *et al.*[22].

The present study focuses on the development of an algorithm for estimating TPW from thermal infrared observations in split-window and UTH products of the INSAT-3D Imager from clear sky over the ocean. The algorithm performance was evaluated on the INSAT-3D Imager observations for the year 2018. The spatial as well as seasonal variability of TPW has been demonstrated for robustness of the algorithm. The quality of the retrieved TPW was evaluated through validation against RS observations, which showed an error of ~0.6 cm at all four study locations. The quality assessment with MODIS and INSAT-3D sounder TPW products showed an error of 0.5 cm throughout the study period.

Detailed analysis of the estimated TPW from INSAT-3D can provide insights to understand the various atmospheric processes. For example, prediction of the onset of the Indian summer monsoon over Kerala coast. The time-series analysis of TPW can give information about the convective systems developing in the atmosphere. Further, the concentration of TPW provides the important atmospheric correction necessary for estimation of accurate surface parameters, e.g. land and sea surface temperatures from satellite observations. The TPW information is also a important input for atmospheric correction in the visible and SWIR channels of the INSAT-3D Imager that is used for estimation of surface albedo, aerosol optical depth, and other land/ocean surface parameters involving the use of these optical channels. The TPW product from the INSAT-3D Imager will provide higher spatial and temporal observations as well as a larger region of observations (full-disk coverage in the Imager versus limited smaller area from the Sounder). This algorithm has also been extended to the INSAT-3DR Imager observations, which will enable observation of TPW from the Imager at every 15 min interval.

1. Yuan, L. L., Anthes, R. A., Ware, R. H., Rocken, C., Bonner, W. D., Bevis, M. G. and Businger, S., Sensing climate change using the global positioning system. *J. Geophys. Res.*, 1993, **98**(D8), 14925; doi:10.1029/93JD00948.
2. Liu, J., Sun, Z., Liang, H., Xu, X. and Wu, P., Precipitable water vapor on the Tibetan Plateau estimated by GPS, water vapor radiometer, radiosonde, and numerical weather prediction analysis and its impact on the radiation budget. *J. Geophys. Res. D*, 2005, **110**(17), 51–61; doi:10.1029/2004JD005715.
3. Manning, T., Zhang, K., Rohm, W., Choy, S. and Hurter, F., Detecting severe weather using GPS tomography: an Australian case study. *J. Global Position. Syst.*, 2012, **11**, 58–70.
4. Lee, S. J., Ahn, M. H. and Lee, Y., Application of an artificial neural network for a direct estimation of atmospheric instability from a next-generation imager. *Adv. Atmos. Sci.*, 2016, **33**, 221–232.
5. Trenberth, K. E., Dai, A., Rasmussen, R. M. and Parsons, D. B., The changing character of precipitation. *Bull. Am. Meteorol. Soc.*, 2003, **84**, 1205–1218.
6. Sobrino J. A., Li, Z. L., Stoll, M. P. and Becker, F., Improvements in the split-window technique for land surface temperature determination. *IEEE Trans. Geosci. Remote Sensing*, 1994, **32**(2).
7. Francois, C. and Ottle, C., Atmospheric corrections in the thermal infrared: global and water vapor dependent split-window algorithms–applications to ATSR and AVHRR data. *IEEE Trans. Geosci. Remote Sensing*, 1996, **34**(2), 457–470.
8. Guillory, A. R., Jedlovec, G. J. and Fuelber, H. E., A technique for deriving column-integrated water content using VAS split-window data. *J. Appl. Meteorol.*, 1993, **32**, 1226–1241.
9. Kleespies, T. J. and McMillin, L. M., Retrieval of precipitable water from observations in the split window over varying surface temperatures. *J. Appl. Meteorol.*, 1990, **29**, 851–862.
10. Chesters, D., Uccellini, L. W. and Robinson, W. D., Low-level water vapor fields from the VISSR Atmospheric Sounder (VAS) 'split-window' channels. *J. Climate Appl. Meteorol.*, 1983, **22**, 725–743.
11. Chesters, D., Robinson, W. D. and Uccellini, L. W., Optimized retrievals of precipitable water from the VAS 'split-window'. *J. Climate Appl. Meteorol.*, 1987, **26**, 1059–1066.
12. INSAT-3D algorithm theoretical basis document, Space Application Centre, ISRO, Ahmedabad, May 2015; https://mosdac.gov.in/data/doc/INSAT-3D_ATBD_May_2015.pdf
13. Prabhakara, C., Dalu, G. and Kunde, V. G., Estimation of sea surface temperature from remote sensing in 11–13 μm window region. *J. Geophys. Res.*, 1974, **79**, 5039–5044.
14. Eyre, J. R., A fast radiative transfer model for satellite sounding systems. ECMWF Technical Memorandum 176, 1991.
15. Saunders, R. W., Matricardi, M. and Brunel, P., An improved fast radiative transfer model for assimilation of satellite radiance observations. *Q. J. Royal Meteorol. Soc.*, 1999, **125**, 1407–1425.
16. Matricardi, M., Chevallier, F. and Tjemkes, S., An improved general fast radiative transfer model for the assimilation of radiance observations. ECMWF Technical Memorandum 345, 2001.
17. Chevallier, F., Michele, S. D. and McNally, A. P., Diverse profile datasets from the ECMWF 91-level short-range forecast. NWPSAF-EC-TR-010, 2006.
18. Thapliyal, P. K., Shukla, M. V., Shah, S., Joshi, P. C., Pal, P. K. and Ajil, K. S., An algorithm for the estimation of upper tropospheric humidity from Kalpana observations: methodology and validation. *J. Geophys. Res.*, 2011, **116**, D01108; doi:10.1029/2010JD014291.
19. Seemann, S. W., Borbas, E. E., Li, J., Menzel, W. P. and Gumley, L. E., MODIS atmospheric profile retrieval algorithm theoretical basis document, 2006; https://modisimages.gsfc.nasa.gov/_docs/MOD07MYD07ATBDC005.pdf
20. Simon, B., Rahman, S. H. and Joshi, P. C., Conditions leading to the onset of the Indian monsoon: a satellite perspective. *Meteorol. Atmos. Phys.*, 2006, **93**, 201–210.
21. Parihar, S., Mitra, A. K., Mohapatra, M. and Bhatla, R., Potential of INSAT-3D sounder-derived total precipitable water product for weather forecast. *Atmos. Meas. Tech.*, 2018, **11**, 6003–6012.
22. Rao, V. K., Mitra, A. K., Singh, K. K., Bharathi, G., Kumar, R. R., Ray, K. and Ramakrishna, Ssvs., Evaluation of INSAT-3D derived TPW with AIRS retrievals and GNSS observations over the Indian region. *Int. J. Remote Sensing*, 2019, doi:10.1080/01431161.2019.1657604.